

# Factors Controlling the Enhanced Mechanical and Thermal Properties of Nanodiamond-Reinforced Cross-Linked High Density Polyethylene

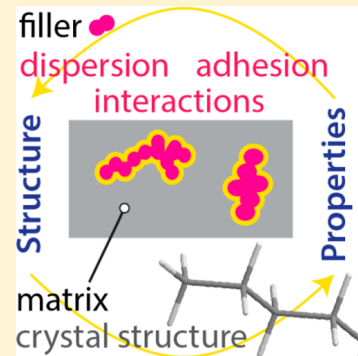
Eleftheria Roumeli,<sup>\*,†</sup> Eleni Pavlidou,<sup>†</sup> Apostolos Avgeropoulos,<sup>§</sup> Georgios Vourlias,<sup>†</sup> Dimitrios N. Bikaris,<sup>‡</sup> and Konstantinos Chrissafis<sup>\*,†</sup>

<sup>†</sup>Solid State Physics Department, and <sup>‡</sup>Laboratory of Polymer Chemistry and Technology, Department of Chemistry, Aristotle University of Thessaloniki, Thessaloniki 541424, Greece

<sup>§</sup>Polymers' Laboratory, Department of Materials Science Engineering, University of Ioannina, University Campus, Ioannina 45110, Greece

## Supporting Information

**ABSTRACT:** A systematic investigation of the factors influencing the notable enhancement of the mechanical and thermal properties of nanodiamonds (NDs)-reinforced cross-linked high density polyethylene (PEX) is presented in this work. The effects of crystal structure and molecular conformation as well as filler dispersion and adhesion with the matrix were found to govern the mechanical properties of the final composites. A considerable increase in the strength, toughness, and elastic modulus of the materials was found for the composites with filler content below 1 wt %. For higher NDs concentrations, the properties degraded. When filler concentration does not exceed 1 wt %, enhanced adhesion with the matrix is achieved, allowing a more successful load transfer between the filler and the matrix, thus enabling an effective reinforcement of the composites. The higher degree of crystallinity along with larger crystal size are also positively influencing the mechanical properties of PEX. Higher filler concentrations, on the other hand, lead to the formation of larger aggregates, which lead to lower adhesion with the matrix, while they also constitute stress concentrators and therefore reduce the positive reinforcement of the matrix. The thermal conductivity of the composites was also found to be significantly increased for low-filler concentrations. This enhancement was less significant for higher NDs concentrations. It is concluded that this reinforcement is due to the heat capacity increase that NDs incorporation causes in PEX. Additionally, a thermal stability enhancement was found for the composite with minimum filler content.



## 1. INTRODUCTION

Polymer nanocomposites represent a class of materials that during the past years have attracted the attention of both academic and industrial research communities. These multi-component systems have showed important property enhancements with exceedingly low nanofiller amounts.<sup>1,2</sup> Even though the scientific community has put on a lot of effort to understand and be able to predict the behavior of nanocomposites, their properties and performance are far from being comprehended. It is common belief though that efforts for fundamental understanding of the factors influencing nanocomposites' final properties are essential and should always be encouraged.

During the past years, significant efforts have been made to understand the influence of crystal structure and morphology along with molecular conformation and weight distribution, crystallization conditions, and thermomechanical history effects on the properties of polymers.<sup>3–6</sup> For composites and nanocomposites in particular, the filler state, dispersion, morphology, and adhesion with the matrix have gained much attention as they strongly affect the final reinforcement of the composites.<sup>7–9</sup> Systematic investigations of microstructure

property relationships in nanocomposites have also found great response.<sup>10–14</sup> After such a study has been performed, the corresponding hybrids or composites could be redesigned to yield materials of specific performance. Still though, fundamental reports on matrix and filler-related factors influencing nanocomposites' reinforcement are rather rare, and even more so in polymer nanocomposites.

In the present work, the mechanical and thermal properties reinforcement of silane cross-linked high density polyethylene was pursued. PEX was chosen as a matrix because it is a widely produced industrial polymer with great mechanical properties, used in a variety of applications including hot water and geothermal piping installations, wires, and cables.<sup>15,16</sup> With the chemical or physical cross-linking process, polyethylene undergoes a structural change that improves many of its features such as operating temperature, abrasion, chemical resistance, and mechanical performance through time<sup>17</sup> and results in a superior-performance material, suitable for such

**Received:** May 8, 2014

**Revised:** September 9, 2014

**Published:** September 9, 2014

high-demanding applications. Thus, the enhancement of its mechanical as well as thermal properties is greatly important for the polymer industry and has been the main goal of the present research along with the comprehension of the observed reinforcement.

In our previous works,<sup>18,19</sup> multiwalled carbon nanotubes were selected and tested for the mechanical and thermal properties reinforcement of PEX. In the present research, nanodiamonds that represent a carbon form that combines all of the benefits of nanoscale-fillers with the well-known superior diamond properties including exceptional hardness and elastic modulus<sup>20–22</sup> were selected toward the same goal. Furthermore, it is well-known that NDs have almost the highest thermal conductivity among conductive fillers and their addition into PEX could increase its thermal conductivity. Recent research on polymer–NDs composites has proved that NDs can be a promising reinforcing agent, which could enable the superior performance of various polymer matrixes in versatile applications like engineering,<sup>23</sup> coatings,<sup>24</sup> lubricants,<sup>25,26</sup> as well as several others.<sup>27–29</sup>

Depending on the targeted application, NDs may require an extensive pretreatment, such as surface functionalization.<sup>30–32</sup> Many groups have presented significant findings on how the rich surface chemistry of NDs can drastically improve the particles dispersion and subsequently the reinforcement of the hosting matrix.<sup>33–38</sup> Noteworthy achievements in this field include the covalent grafting of various functional groups and molecules on the top of chemical vapor deposition diamond films,<sup>39–41</sup> as well as the absorption of organic molecules, small macromolecules, or even highly complex structures like DNA or enzymes from the different surface termination groups on the diamond surface.<sup>42–45</sup> Such insightful ways to functionalize diamond have inspired numerous surface modification approaches for diamond particles in the nanoscale, which have already led to significant innovations in applications like drug delivery, photostable fluorescence labeling, magnetooptic sensorring, and several others.<sup>46–51</sup>

Even though surface functionalization is a hopeful prospect toward successfully incorporating NDs into a hosting matrix, in the present work we evaluated an alternative approach to achieve the successful reinforcement of the selected polymer matrix. 0.5–5 wt % NDs were incorporated into PEX first by mechanical processing (solid-state ball milling) and then by melt rheomixing. Mechanical milling has proven to be a promising alternative to surface modification,<sup>52–54</sup> along with other mechanical deagglomeration approaches such as sonication and stirring.<sup>55,56</sup> The solid-state ball milling approach was selected as it is considered a cost-effective alternative method, which can easily be adopted by the plastics manufacturing industry.

The tensile properties of the prepared nanocomposites were measured, and the effects of NDs on the crystal structure and morphology of PEX as well as filler dispersion and adhesion were among the investigated factors influencing the mechanical behavior of the composites. Moreover, the composites' thermal properties significant enhancement was monitored and evaluated through various techniques.

## 2. EXPERIMENTAL SECTION

**2.1. Materials.** High density polyethylene grafted with vinyl trimethoxysilane (g-HDPE) was kindly supplied by Sioplas S.A. and exhibited the following characteristics: average molecular weight per number,  $\bar{M}_n = 28\,000$  g/mol; average molecular

weight per weight,  $\bar{M}_w = 120\,200$  g/mol; and intrinsic viscosity,  $[\eta] = 1.54$  dL/g. A catalyst masterbatch containing the same polymer along with dibutyltin dilaurate (DBTDL), internal lubricants, stabilizers, and various antioxidants was also supplied by Sioplas S.A. Nanodiamonds powder was purchased from International Technology Center (NC) with an average primary particle size equal to 4.0 nm and purity >98%.

**2.2. Nanocomposites' Preparation.** Prior to melt mixing, solid-state ball milling was employed to achieve a fine dispersion of the NDs in the polymer matrix. Mixtures of 95 parts of g-HDPE, 5 parts of catalyst masterbatch, and 0.5, 1, 3, and 5 wt % NDs were solid-state mixed for 6 h in a Retsch centrifugal ball mill (model S 100). A cylindrical stainless steel jar of 50 mL with six steel balls of 10 mm in diameter was used, and a rotation speed of 500 rpm was applied. Each mixture after ball milling was melt-mixed in a Haake–Buchler rheomixer (model 600) with roller blades and a mixing head with a volumetric capacity of 69 cm<sup>3</sup>. During the mixing period, the melt temperature and torque were continuously recorded. For this case, a 10 min mixing at 200 °C with a torque speed of 60 rpm was used. The prepared samples were immediately hot pressed using an Otto Weber, type PW 30 hydraulic press connected with an Omron ESAX temperature controller, at a temperature of 180 ± 5 °C, to prepare films of 10–30 μm and 350–450 μm thickness appropriate for each type of measurement. The films were rapidly cooled by immersion in water at 25 °C. Finally, all prepared films were exposed to a hot bath (90 °C water for 24 h) to complete the cross-linking process in the bulk of the polymer as previously reported.<sup>57</sup>

**2.3. Methods.** **2.3.1. Mechanical Properties.** Mechanical properties testings were performed on an Instron 3344 dynamometer, in accordance with ASTM D638 using a cross-head speed of 50 mm/min. Sheets of about 350–450 μm thickness were used, prepared as described previously. To measure the mechanical properties from these sheets, dumbbell-shaped tensile test specimens (central portions 5 × 0.5 mm thick, 22 mm gauge length) were cut in a Wallace cutting press. At least five measurements were conducted for each sample, and the results were averaged to obtain a mean value. The values of elastic modulus, tensile strength at yield and at break point, and elongation at break were determined. The toughness was calculated from the area under the obtained stress-strain curves as described elsewhere.<sup>58</sup>

**2.3.2. Transmission Electron Microscopy (TEM).** The dispersion of NDs was examined by transmission electron microscopy (TEM) images that were taken from thin film sections of the various nanocomposites through cryo-microtoming at -90 °C with a DIATOME cryo-45° diamond knife by the ultramicrotome Leica EM FC7. The thin sections were deposited on copper grids. TEM micrographs were obtained using a JEOL 120 CX microscope operating at 120 kV.

**2.3.3. Scanning Electron Microscopy (SEM).** The morphology of the prepared tensile specimens was examined in a SEM system (JEOL JSM 840A-Oxford ISIS 300 microscope). The samples were carbon coated to provide good conductivity of the electron beam. Operating conditions were: accelerating voltage 20 kV, probe current 45 nA, and counting time 60 s.

**2.3.4. Differential Scanning Calorimetry (DSC).** DSC measurements have been performed in a DSC141 (Setaram). Six milligrams of each sample were placed in an aluminum sealed crucible, while an identical empty crucible was used as reference in each measurement. The samples were heated at 5 °C/min from ambient temperature to 200 °C, held at 200 °C

for 5 min, cooled to 60 °C with a cooling rate of 5 °C/min, and then heated again with the same heating rate. The second heating data were used for analysis in the present work.

**2.3.5. X-ray Diffraction (XRD).** X-ray diffraction patterns of the prepared materials (10–30 μm thick) were recorded by a water-cooled Rigaku Ultima<sup>+</sup> diffractometer using Cu K $\alpha$  radiation, a step size of 0.02°, and a step time of 3 s, operating at 40 kV and 30 mA.

**2.3.6. Thermal Conductivity Measurements Using Laser Flash Analysis (LFA) and Temperature Modulated Differential Scanning Calorimetry (TMSDC).** Thermal conductivity measurements were performed using a laser flash analysis instrument (LFA 457, Netzsch). Samples were cut into (10 × 10) mm squares with 0.4 mm thickness and were coated with 5 μm of graphite. All measurements were taken at 50 °C with a laser voltage power of 2786 V and a laser transmission filter of 100%. A total of 10 shots per sample set were taken. All curves were fitted using a variety of models to determine the most suitable for each material as described previously.<sup>19</sup>

In addition, the heat capacity of each sample was determined by temperature modulated differential scanning calorimetry (DSC Q 200, TA Instruments). The samples were heated from 25 to 95 °C with an underlying heating rate of 2.5 °C/min, modulation amplitude of 0.53 °C, and a period of 80 s. The value of specific heat capacity at 50 °C was obtained for all of the studied materials and used for the determination of thermal conductivity. The thermal conductivity specifically at 50 °C was selected as an intermediate operating temperature in a geothermal piping system.

**2.3.7. Thermogravimetry (TG).** Thermogravimetric (TG) analysis was carried out with a Setsys 16/18 TG-DTA (Setaram). Samples ( $4 \pm 0.2$  mg) were placed in alumina crucibles. An empty alumina crucible was used as reference. Samples were heated from ambient temperature to 600 °C at 20 °C/min in a 50 mL/min flow of N<sub>2</sub>.

**2.3.8. Pyrolysis–Gas Chromatography–Mass Spectroscopy (Py–GC–MS).** For Py–GC–MS analysis of PEX and its nanocomposites, a very small amount of each material was placed initially into the Multi-Shot EGA/PY-3030D pyrolyzer (Frontier Laboratories Ltd., Fukushima, Japan). For pyrolysis analysis (flash pyrolysis), each sample was placed into the sample cup, which afterward fell free into the pyrolyzer furnace. The preselected pyrolysis temperature, after TG results evaluation, was 420 °C, and the GC oven temperature was programmed from 50 to 420 °C at 20 °C/min. The sample vapors generated in the furnace were split (at a ratio of 1/50); a portion moved to the column at a flow rate of 1 mL/min, and the remaining portion exited the system via the vent. The pyrolyzates were separated in the Ultra Alloy metal capillary column (UA<sup>+</sup>S) and analyzed by the MS detector GC-MS-QP2010 Ultra (Shimadzu).

**2.3.9. Contact Angle Measurements.** The water and diiodomethane (CH<sub>2</sub>I<sub>2</sub>) contact angle measurements of the prepared materials were performed at room temperature by the sessile drop method using a goniometer PGX (Fibro Systems AB). The values presented in this work are the arithmetic mean of six measurements ( $\pm$ standard deviation). Subsequent specific free energy analysis was performed as described in the corresponding section.

**2.3.10. Fourier Transform Infrared Spectroscopy (FTIR).** FTIR spectra of the NDs were obtained with a Spectrum 1000 Perkin-Elmer spectrometer in the spectral range 4000–400 cm<sup>-1</sup>, with 2 cm<sup>-1</sup> resolution and 32 scans.

### 3. RESULTS AND DISCUSSION

**3.1. Morphology of NDs and Nanocomposites.** In Supporting Information Figure 1, the FTIR spectrum of the as-received NDs is presented. The presence of surface carbonyl, hydroxyl, and oxygen groups on the diamond particles is evident, even though no chemical treatment was employed in this work. The observed pre-existing surface groups could have been formed during the production and storage of NDs or even during their exposure to ambient conditions throughout the preparation of the nanocomposites.

In Figure 1 are presented the TEM images of all prepared nanocomposites. An overall acceptable dispersion was revealed for all of the prepared composites, especially for those with filler content below 1 wt %. Even though aggregates formation could not be avoided in any case, their size does not exceed 100–150 nm for the composites with up to 1 wt % NDs. The composites with 3–5 wt % NDs present an overall acceptable filler dispersion, which is poorer than that found in the composites with lower filler contents. The dimensions of the formed aggregates range between 65 and 375 nm for the PEX/3 wt % NDs composite, and 80–400 nm for the PEX/5 wt % NDs composite. Therefore, TEM images revealed that increasing filler concentrations leads to larger aggregates and also to inferior dispersion. The low filled composites are consequently expected to present a more significant reinforcement as compared to the more heavily filled ones. While the observed filler dispersion may support a reinforcement of the mechanical properties on the lower filler concentrations, other factors, such as adhesion and possible interactions between the filler and the matrix, must be considered for reliable conclusions.

**3.2. Mechanical Properties of the Nanocomposites.** In Figure 2 are presented characteristic stress–strain curves of all of the samples. From these experiments, it can be concluded that the presence of NDs has a great impact on the mechanical performance of PEX. An initial stiffness increase for the low filler concentrations can be distinguished, which decreases with increasing filler content. Furthermore, a clear reduction of ductility with increasing NDs loading can also be observed. Even though the fracture behavior of the composites with NDs content higher than 3 wt % does not qualify as brittle, the decreased strain prior to failure along with the reduction of the stress at break values marks a noteworthy decrease in their ductility. In that aspect, the composites with higher filler loading experience an embrittlement. This also explains the lower toughness of these composites. In Table 1 are presented averaged values of all of the measured properties.

A great enhancement of more than 150 MPa on the elastic modulus of PEX is obtained from the incorporation of 0.5 wt % NDs, while for higher NDs concentrations this increase progressively levels off, but remains 70–100 MPa higher when compared to neat PEX. For the stress at yield point the maximum enhancement exceeds 7.5 MPa and was also achieved with the lowest filler loading, while for the higher concentrations it levels off at approximately 22.2 MPa, remaining in any case higher than neat PEX. The stress at break however is significantly enhanced for the composites with 0.5–1 wt % NDs and is lower than the neat PEX for the higher concentrations. The noteworthy enhancement of the strength at break is almost 45% for the PEX/0.5 wt % NDs composite. Similarly, the elongation at break and toughness are enhanced for the composites with the lowest amount of NDs, and then they decrease for higher filler loadings. The toughness

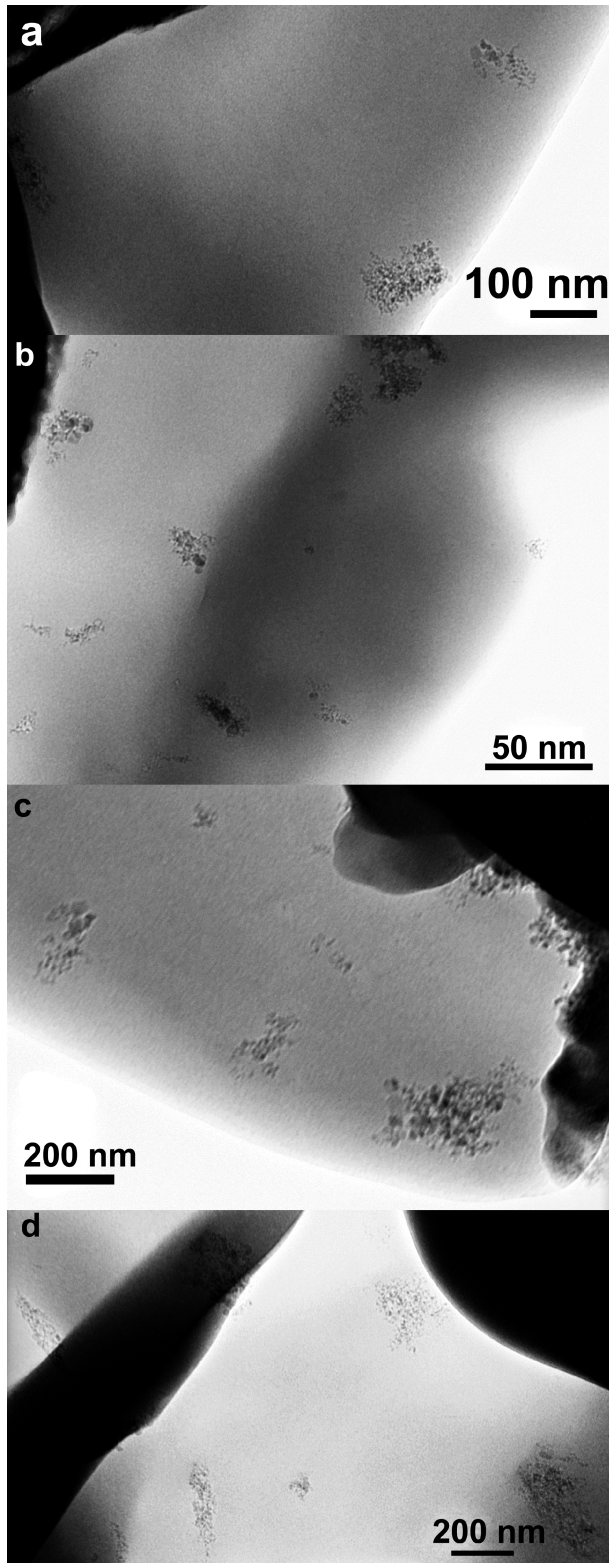


**Figure 1.** TEM images of (a) PEX/0.5 wt % NDs, (b) PEX/1 wt % NDs, (c) PEX/3 wt % NDs, and (d) PEX/5 wt % NDs.

enhancement is higher than  $320 \text{ J/m}^3$  for the composite with lowest NDs content. The observed embrittlement of PEX as a consequence of increasing NDs content has also been reported by other groups in the literature.<sup>59–61</sup>

**3.3. Fractography Studies.** As the nanocomposites exhibit a transition in their fracture behavior, from ductile to less

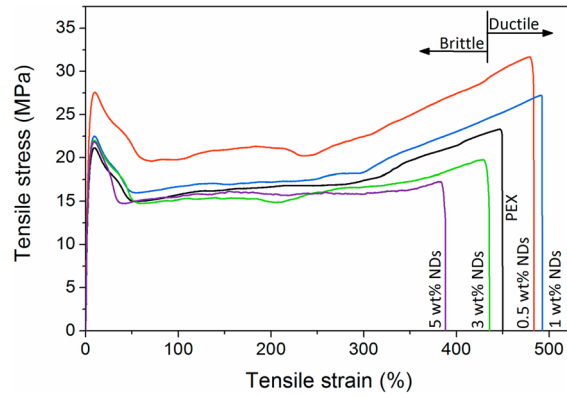


**Figure 2.** Stress-strain curves of PEX and its nanocomposites with NDs.

ductile or brittle-like, the investigation of their failure surfaces by means of fractography was considered crucial.

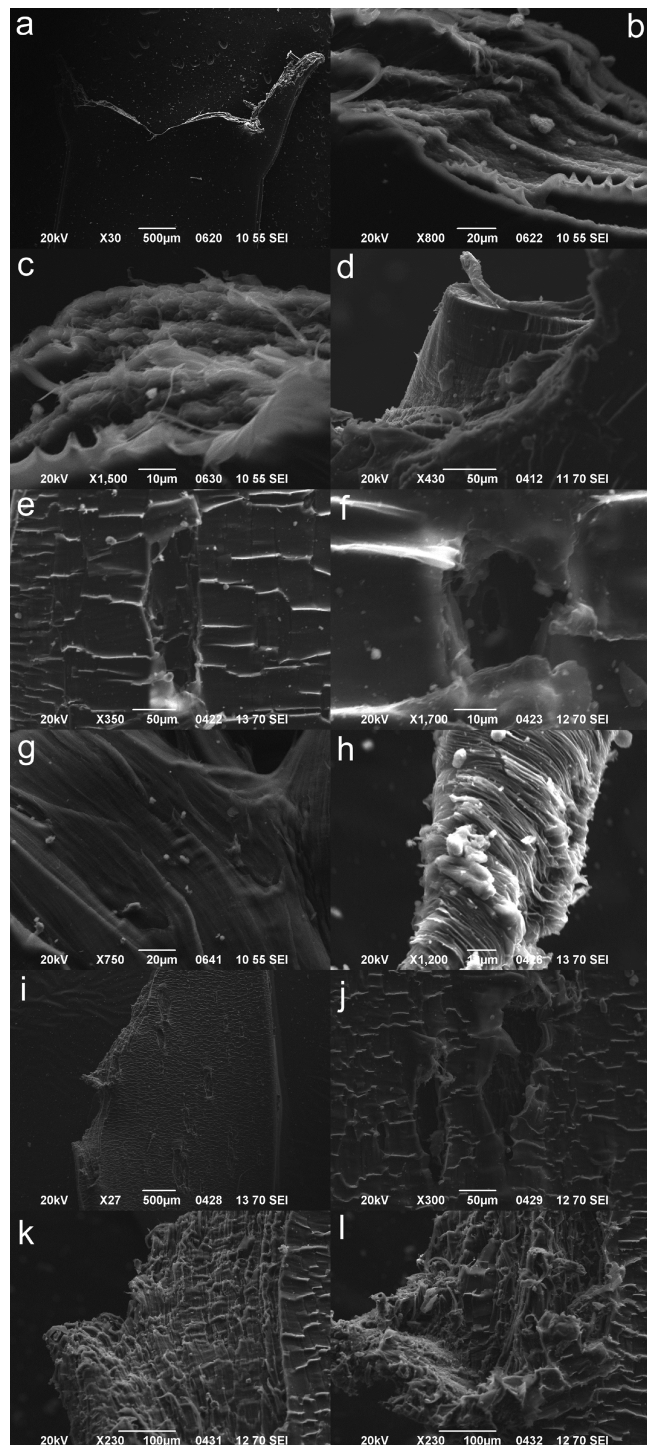
Polymeric materials have either brittle or ductile performance according to various parameters including their crystallinity, molecular weight distribution, and processing temperature, among others. As previously reported from our studies on neat PEX,<sup>18</sup> it is considered ductile as it involves a considerable plastic deformation prior to failure. The evolution of the process includes material's necking, void coalescence, and crack propagation, and it is terminated by a final shear fracture through fibrillar pull-out, indicating the amount of plastic deformation. In nanocomposites, however, differences in the materials' fracture are expected. Local disruptions of the material's order, like density or concentration fluctuations and filler aggregations, can act as stress concentrators leading to premature failure. Therefore, it is expected that large NDs aggregates, which were found through TEM images in the composites with filler loading higher than 3 wt %, may act as stress concentrators leading to premature failure.

From the SEM observations of the 0.5–1 wt % NDs containing composites presented in Figure 3a–d, their highly ductile fracture can be seen. The exterior of the specimens appears rather smooth, with a few shallow microcracks, but no deep microvoids or crack coalescence signs can be observed. Moreover, the dense and uniform fibrillar structure of the polymer is retained in these composites, and it suggests that the fibrils have withstood an undisputed deformation. The high degree of deformation that these composites have experienced can be revealed through the drawn ultrathin polymer fibrils shown in these images. A closer inspection of the composites' surfaces reveals that the dominant deformation mechanism is shear banding, which provides more efficient energy dissipation than crazing.<sup>62</sup> The SEM images of the composite with 3–5 wt % NDs are presented in Figure 3e–l, and they reveal a more damaged surface exhibiting many deep micro- and macro-cracks. Besides the apparently rougher surface, these composites have clearly experienced a lower degree of deformation prior to failure, as denoted by their more abruptly failed fibrils. In Figure 3e,f, the progressed crack coalescence that led to failure can clearly be seen in the PEX/3 wt % NDs composite. However, the deformation mechanism is still shear banding as evidenced from Figure 3g,h.

In conclusion, the observation of the failure surfaces of the composites reveals distinct differences in those with loading higher than 1 wt %. The notably smaller extent of deformation that these composites have experienced is in agreement with

**Table 1.** Mechanical Properties of the Prepared Nanocomposites

NDs, wt %	elastic modulus, MPa	stress at yield, MPa	stress at break, MPa	elongation at break, %	toughness, J/m <sup>3</sup>
0	675 ± 35	19.8 ± 0.7	22.0 ± 2.0	420.0 ± 21.0	1893 ± 150
0.5	830 ± 50	27.6 ± 2.5	31.7 ± 2.5	495.5 ± 15.0	2221 ± 200
1	776 ± 22	24.9 ± 1.5	27.2 ± 0.5	472.2 ± 25.0	2061 ± 55
3	747 ± 15	22.1 ± 0.5	19.6 ± 2.3	453.3 ± 40.0	1827 ± 135
5	748 ± 15	22.3 ± 1.0	16.7 ± 0.9	378.6 ± 15.0	1345 ± 40

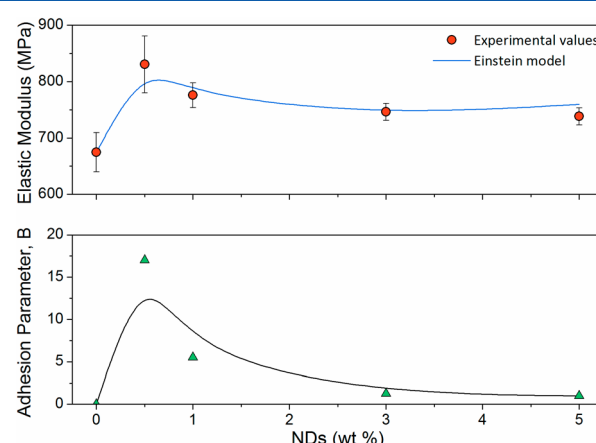
**Figure 3.** SEM images of the fracture surface of PEX with (a,b) 0.5, (c,d) 1, (e–h) 3, and (i–l) 5 wt % NDs.

their lower ductility and toughness, which was found through the tensile testings.

**3.4. Interfacial Adhesion and Filler–Matrix Interactions Effects on the Mechanical Properties of PEX/NDs Nanocomposites.** In general, the superior stiffness of NDs can benefit the composites' modulus and strength at yield performance when filler dispersion is fine. Moreover, adhesion between nanofillers and the polymer matrix also leads to improved stiffness,<sup>7,63</sup> which can be confirmed by applying the Einstein equation:

$$\frac{E_c}{E_m} = 1 + BV_f \quad (1)$$

where  $E_c$  and  $E_m$  are the elastic moduli of the composite and the polymer matrix respectively,  $V_f$  is the volume fraction of the filler, and  $B$  is a constant related to interfacial adhesion. When no adhesion exists between the matrix and the fillers,  $B$  becomes 1, while for strong adhesion,  $B$  becomes higher than 2.5.<sup>7</sup> In the present work, the values of elastic modulus of the composites indicate that the adhesion between PEX and NDs may vary with filler content. In Figure 4, the satisfactory fitting

**Figure 4.** Elastic modulus experimental and fitted values using Einstein's model and adhesion parameter variation against NDs concentration.

of experimental data using Einstein's model and the variation of adhesion parameter with nanofiller content are illustrated. It can clearly be seen that significant adhesion is achieved for the low filler concentrations, while as the NDs loading increases, the adhesion decreases, which is in agreement with the observed decrease of the composites' stiffness. The noteworthy interfacial adhesion observed in the two composites with lower filler concentration can be correlated with the smaller aggregates found through TEM observations in these systems (Figure 1). In fact, the ratio of present to available surface functional groups of NDs is expected to be decreasing as we move from dispersed single particles to small, medium, and

**Table 2.** Contact Angles and Specific Free Energy Calculations Using Fowkes' and Wu's Methods for All of the Prepared Nanocomposites

NDs (wt %)	contact angle (deg)		Fowkes specific free energy contributions ( $J/m^2$ )			Wu specific free energy contributions ( $J/m^2$ )		
	water	$CH_2I_2$	total	dispersive	polar	total	dispersive	polar
0	$80.4 \pm 3.8$	$55.4 \pm 3.3$	$32.7 \pm 4.4$	$25.6 \pm 2.2$	$7.3 \pm 2.2$	$39.2 \pm 3.4$	$27.7 \pm 1.5$	$11.6 \pm 1.8$
0.5	$99.8 \pm 4.8$	$59.7 \pm 2.6$	$28.3 \pm 3.2$	$27.5 \pm 2.3$	$0.8 \pm 0.9$	$30.8 \pm 3.6$	$27.1 \pm 1.7$	$3.7 \pm 1.9$
1	$102.5 \pm 4.5$	$56.0 \pm 1.6$	$30.5 \pm 2.2$	$30.3 \pm 1.8$	$0.3 \pm 0.5$	$31.7 \pm 3.4$	$29.3 \pm 1.7$	$2.4 \pm 1.8$
3	$107.0 \pm 2.1$	$49.1 \pm 1.5$	$36.8 \pm 1.3$	$36.7 \pm 1.2$	$0 \pm 0.1$	$37.4 \pm 6.2$	$37.7 \pm 5$	$-0.3 \pm 1.2^a$
5	$106.8 \pm 2.3$	$54.1 \pm 1.5$	$33.3 \pm 1.2$	$33.3 \pm 1.2$	$0 \pm 0$	$33.5 \pm 3.5$	$33.2 \pm 2.5$	$0.4 \pm 1$

<sup>a</sup>Negative contributions are considered as zero.

large aggregates. Therefore, as evidenced from the collected TEM images, the low-filled composites have smaller and better dispersed NDs aggregates, which implies that more surface groups would be available to contribute to a better adhesion between the filler and the matrix. As filler concentration increases and larger aggregates are formed, less surface groups would be able to contribute to the adhesion of NDs with PEX. Thus, the rationalized higher interfacial adhesion found in the two composites with lower filler concentration can support the more significant enhancement in the stiffness of these composites. As filler dispersion becomes less sufficient and interfacial adhesion is lower, it is expected that stiffness will follow a similar trend.

In nanocomposite systems, filler–matrix interactions should also be considered as they greatly influence the composites' mechanical performance.<sup>9</sup> Toward that aspect, contact angle measurements and subsequent surface tension and interactions analysis were performed. Using the liquid–solid surface interaction parameters, as an indication of the intermolecular filler–matrix interactions, the results, presented in Table 2, support the tensile testing findings.

Analysis of the obtained measurements was performed using the most widely accepted processes. Starting from Young's expression,<sup>64</sup> the measured contact angle ( $\theta$ ) was related to the specific free energy of the solid ( $\gamma_s$ ) and the used liquid ( $\gamma_L$ ) with the interfacial free energy between the solid and the liquid ( $\gamma_{SL}$ ):

$$\gamma_L \cos \theta = \gamma_s - \gamma_{SL} \quad (2)$$

Because various forces exist within the matrix (including its interactions with the filler) like polar, dispersive, and hydrogen-bonding forces, among others, a variety of models have been developed during the past decades for the determination of  $\gamma_s$  taking into account all of these effects. One of the most thorough approaches was proposed by Wu,<sup>65</sup> combining a harmonic mean equation of the polar and dispersive forces found in polymer matrixes:

$$(1 + \cos \theta_L) \gamma_L = 4 \left[ \frac{\gamma_L^d \gamma_s^d}{\gamma_L^d + \gamma_s^d} + \frac{\gamma_L^p \gamma_s^p}{\gamma_L^p + \gamma_s^p} \right] \quad (3)$$

where the subscript "L" is for the liquid used in the measurement, and the superscripts "d" and "p" correspond to the dispersive and polar components of the specific free energy, respectively.

The total specific free energy ( $\gamma_s$ ) is the sum of its polar and dispersive components. To perform such an experiment, liquids of different polarities ought to be used, and in the present case water and  $CH_2I_2$  were employed with literature reported data for their surface energy components.<sup>66</sup>

Moreover, the work of adhesion ( $W_A$ ) was calculated from the expression:

$$W_A = \gamma_L (1 + \cos \theta) \quad (4)$$

The interfacial free energy was calculated from Dupre's equation:<sup>67</sup>

$$\gamma_{SL} = \gamma_s - \gamma_L - W_A \quad (5)$$

The spreading coefficient ( $S_c$ ) was obtained from the expression:<sup>68</sup>

$$S_c = \gamma_s - \gamma_{SL} - \gamma_L \quad (6)$$

Also, Girifalco–Good's interaction parameter ( $\varphi$ ) was determined from the following equation:<sup>69</sup>

$$\varphi = \frac{\gamma_L (1 - \cos \theta)}{2 \sqrt{\gamma_s \gamma_L}} \quad (7)$$

From the progressive increase in water contact angle, it was established that the weak hydrophilic nature of PEX converts to hydrophobic as NDs concentration increases. From the dispersive contact angle measurements, a small variation of  $10^\circ$  with an initially decreasing trend for 0.5–3 wt % NDs was observed. A rather interesting effect was found regarding the specific free energy of the composites, as shown from the results of Table 2 using both methods. The balance between polar and dispersive forces contribution is significantly affected by the presence of NDs. While in the neat polymer, polar forces present in the matrix through the Si–O, C–O, and O–H bonds, correspond to 20–30% of the total specific free energy, they drastically decrease to almost zero as NDs content increases. Meanwhile, the dispersive forces contribution is enhanced as a consequence of filler content.

The significant impact of NDs on the surface properties of PEX is further highlighted though the interaction parameter calculations according to Girifalco–Good's method as illustrated in Figure 5. The polar interaction parameter that appears to be almost constant with NDs concentration cannot be taken into consideration in the present case, as polar forces are almost extinct in the composites. Therefore, only the nonpolar medium calculations can be taken into account. Indeed, the dispersive interactions parameter presents a decreasing trend with increasing filler loading. Especially for the composites with NDs content higher than 3 wt %, the interaction parameter values were lower than that of neat PEX, which is in agreement with the observed ultimate strength and toughness behavior. Thus, the interactions between NDs and the matrix appear to be higher for lower filler content (below 1 wt %) and lower for higher filler loadings, suggesting a more pronounced strength and toughness enhancement on the low-filled composites. The correlation between the toughness and the calculated

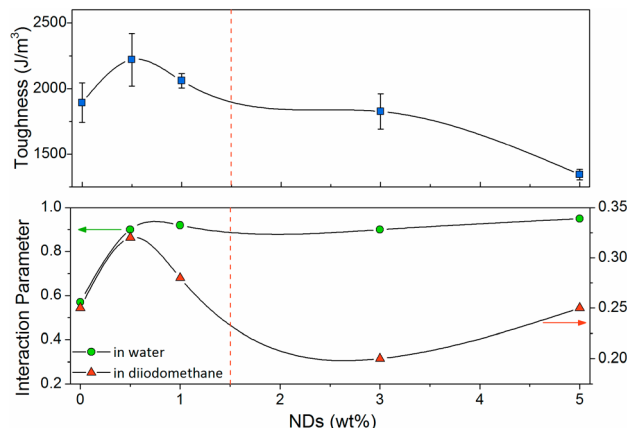


**Figure 5.** Correlation of interaction parameters with toughness in the prepared materials.

interaction parameters is illustrated in Figure 5 (similar correlation is found with the strength at break dependence). The behavioral transition has been highlighted by the red dashed line, supporting the positive effect of higher filler–matrix interactions on the toughness of the composites, which is reduced when interactions are lower. The fact that these interactions are superior in the composites with lower filler content is another indication that higher filler concentrations lead to larger aggregates, which have inferior interactions with the matrix. This result is in agreement with the previously discussed brittleness of the higher filler loaded composites.

**3.5. Crystal Structure and Molecular Conformation Effects on Tensile Strength and Toughness.** Crystal features of the matrix such as crystallinity and spherulite size may be directly correlated to the elastic modulus enhancement of reinforced polymers.<sup>70</sup> However, the behavior of nanocomposites is never a simple function of crystallinity and crystal structure, and other factors such as crystal thickness, crystallization conditions, and interfacial interactions should also be considered.

The examination of crystal structure of the prepared materials was performed using XRD and DSC. Polyethylene crystallizes in orthorhombic system (space group *Pnam*), but in its diffraction patterns the peaks corresponding to (110), (200), and (020) crystallographic planes are the ones that can be clearly distinguished.<sup>71,72</sup> Therefore, mainly the variations of *a* and *b* unit cell parameters along with the *d*<sub>110</sub> and *d*<sub>200</sub> interplanar spacings can be studied. The calculated values that resulted from XRD refinement are presented in Table 3, and they mark a notable effect of NDs on the crystal structure of PEX. Indeed, the presence of NDs results in an overall increased average unit cell and *d*-spacings. However, a specific trend in the observed increases was not detected. Thus, the presence of NDs leads to somewhat larger unit cells and slightly

higher interplanar distances. This finding can be rationalized by taking into account that the induction of NDs into PEX results in the formation of large stress fields within the matrix, around which the polyethylene crystallites are likely to be affected. In this case particularly, the NDs aggregates seem to have forced an enlargement of the crystals formed in their surrounding area, and these enlarged crystals contribute to the overall higher unit cell and *d*-spacing values of the nanocomposites.

Moreover, from the ratio of the crystalline peaks area over the total diffraction area, the degree of crystallinity ( $\omega_c$ ) can be obtained.<sup>73</sup> As can be seen from the values reported in Table 3, the incorporation of 0.5–1 wt % NDs results in an increased degree of crystallinity (approximately 14–15%), while for higher NDs loading crystallinity decreases but remains at least 6% higher than neat PEX at all cases. An increased crystallinity induced by the presence of NDs has also been reported by other groups in the literature.<sup>23,38,59</sup> This fact suggests that small amounts of NDs may act as nucleating agents leading to the formation of more crystals,<sup>74</sup> but when their amount exceeds 1 wt %, this effect is less pronounced. The increased crystallinity of the nanocomposites, which is decreasing with NDs content but remains higher than neat PEX, can also be correlated with their observed enhanced stiffness, in agreement with previous literature reports.<sup>38,59,75</sup>

It has also been proposed that a correlation between crystal thickness and strength at yield can be performed in various semicrystalline polymers and composites.<sup>3,5,6</sup> To obtain the crystal thickness values, the Thomson–Gibbs method was employed,<sup>76</sup> and thus the melting traces of the materials needed to be obtained (Figure 6).

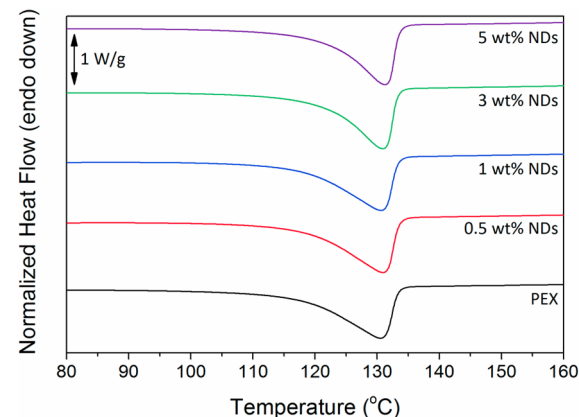


**Figure 6.** DSC curves of PEX and its nanocomposites with NDs.

The crystal thickness ( $L_c$ ) according to the Thomson–Gibbs method can be calculated using the following expression:

$$L_c = \frac{2\sigma_e T_m^0}{(T_m^0 - T_m)\Delta h_f^0 \rho_c} \quad (8)$$

where  $\sigma_e$  is the fold surface free energy ( $9.3 \times 10^{-6}$  J/cm<sup>2</sup> for polyethylene<sup>77</sup>),  $\Delta h_f^0$  is the heat of fusion per unit volume (taken as 293 J/cm<sup>3</sup><sup>78</sup>),  $T_m$  and  $T_m^0$  are the experimental and equilibrium melting peak temperatures, respectively ( $T_m^0$  taken as 145.7 °C<sup>78</sup>), and  $\rho_c$  is the totally crystalline polyethylene density (taken as 1000 kg/m<sup>3</sup><sup>76</sup>).

The amorphous interlayer thickness ( $L_a$ )<sup>79</sup> was also calculated using the following expression:

**Table 3. Crystal Structure Parameters of PEX and Its Nanocomposites with NDs**

NDs (wt %)	$\omega_c$ (%)	<i>a</i> (Å)	<i>b</i> (Å)	<i>d</i> <sub>110</sub> (Å)	<i>d</i> <sub>200</sub> (Å)
0	57.2	7.370	4.935	4.097	3.696
0.5	70.9	7.475	4.956	4.133	3.731
1	72.2	7.451	4.949	4.124	3.723
3	67.8	7.444	4.955	4.124	3.723
5	63.4	7.483	4.968	4.143	3.731

$$L_a = \frac{L_c(1 - \omega_c)}{\omega_c} \frac{\rho_c}{\rho_a} \quad (9)$$

where  $\rho_a$  is the totally amorphous polyethylene density (taken as 855 kg/m<sup>3</sup><sup>76</sup>).

The average crystal thickness ( $l_c$ ) then was calculated using the following formula:<sup>3,5</sup>

$$l_c = \Phi_c D \quad (10)$$

where  $D$  is the lamellar long spacing ( $D = L_c + L_a$ ) and  $\Phi_c$  is the crystal volume fraction, calculated by the following formula:<sup>80</sup>

$$\Phi_c = \rho_a \omega_c [\rho_c(1 - \omega_c) + \rho_a \omega_c]^{-1} \quad (11)$$

As can be seen from Figure 7, the average crystal thickness follows the same decreasing trend with increasing filler content

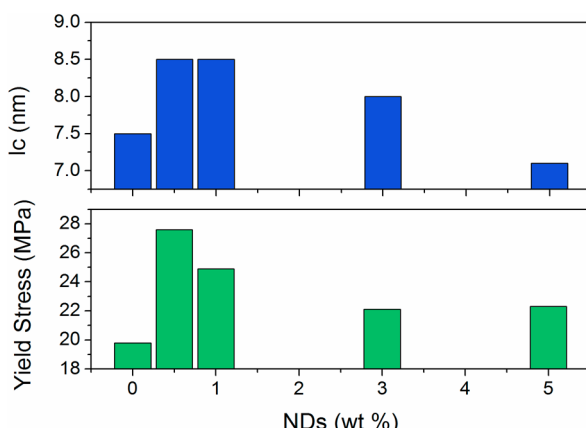


Figure 7. Correlation of yield strength and average crystal thickness for the prepared nanocomposites.

as the yield strength. An initial significant increase is observed for the 0.5–1 wt % NDs, which remains rather high for the 3 wt % composite and levels off as filler content increases further. It has been reported that larger crystals can bear load more efficiently,<sup>58</sup> and therefore the observed linear correlation of the crystal size with yield strength for low filler concentrations can be justified. Only for the PEX/5 wt % NDs is the crystal size lower than that for neat PEX. Thus, for that composite, the smaller crystals that cannot bear load efficiently and constitute tension concentrating points can support the observed lower toughness and premature failure.

**3.6. Thermal Properties of Nanocomposites.** Besides the mechanical properties, enhancement, thermal properties, and specifically thermal conductivity and thermal stability enhancements have also been reported for other NDs-containing polymers.<sup>38,59,61</sup> In Table 4, the thermal diffusivity, specific heat capacity, and thermal conductivity of the prepared composites are presented. A significant thermal conductivity enhancement is observed in all of the composites. The

enhancement is more pronounced in the composite with the lowest filler content, and remains similar to all of the other three composites.

The observed thermal conductivity boost arises almost exclusively from the composites' remarkably enhanced specific heat capacity, which was determined through TMDSC measurements. As can be seen from the results of Table 4, the incorporation of 0.5 wt % NDs in PEX causes a minor increase in the thermal diffusivity, while higher filler concentrations result in values similar to that of the neat polymer. The composite with 5 wt % NDs, however, presents a somewhat decreased thermal diffusivity as compared to the other materials and the neat matrix. On the other hand, 0.5 wt % NDs introduction in PEX results in a 205% higher heat capacity. The higher specific heat capacity of the nanocomposites implies that for the same temperature difference, higher amounts of heat can be absorbed by the nanocomposites as compared to neat PEX. Therefore, the presence of the 0.5 wt % NDs leads to the absorption of higher amounts of heat (to achieve a specific temperature difference in a certain period of time) and slightly enhanced heat transfer through the bulk composite, and, consequently, a 210% higher thermal conductivity. The approximately 100% increased thermal conductivity of the composites with higher filler loadings is a result of their higher heat capacity, as the changes in thermal diffusivity cannot justify their superior thermal conductivity.

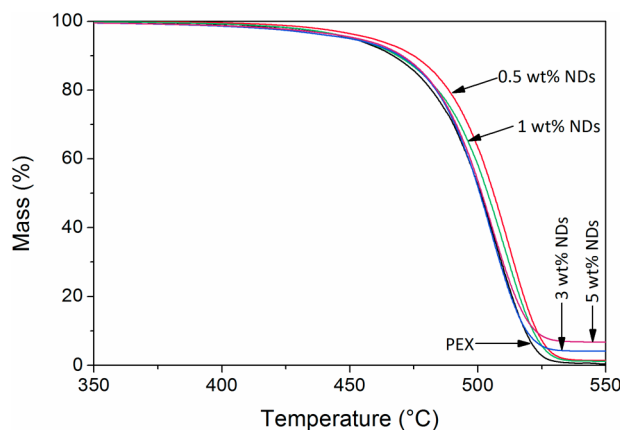
This behavior marks a difference between the use of MWCNTs and NDs as fillers in PEX.<sup>19</sup> As MWCNTs have a larger specific surface area and offer a larger phonon path for heat transfer, they were found to enhance the thermal diffusivity of the matrix as well as its specific heat capacity, resulting in a final thermal conductivity enhancement for the lowest and the highest filler concentration. NDs, on the other hand, offer an even higher increase in the specific heat capacity of the matrix, while they do not really contribute to the thermal diffusivity of the matrix; yet, a comparable, and in the case of 0.5 wt % NDs composite even higher, increase in thermal conductivity of PEX is achieved. Despite this difference, in both of these sets of nanocomposites, the most significant thermal conductivity enhancement was achieved in the lowest filler concentrations. Similar behaviors have also been reported from other groups in literature, concerning different polymer matrixes.<sup>28,61,81</sup> As presented in the previous sections, in the prepared nanocomposites a better dispersion was achieved in the lower NDs concentrations, even though complete particle deagglomeration could not be obtained through the selected preparation route. Additionally, the highest adhesion and filler–matrix interaction parameter values were found also in the composite with lowest filler concentrations. The combination of better dispersion, adhesion, and interactions can therefore explain the highest thermal conductivity of the PEX/0.5 wt % NDs composite. The larger aggregates with lower adhesion and interactions, which were observed in the composites with

Table 4. Thermal Diffusivity, Specific Heat Capacity, and Thermal Conductivity of the Prepared Nanocomposites

NDs (wt %)	thermal diffusivity (mm <sup>2</sup> /s)	specific heat capacity [J/(g·K)]	thermal conductivity [W/(m·K)]
0	0.165 ± 0.001	1.18 ± 0.09	0.17 ± 0.02
0.5	0.173 ± 0.001	3.60 ± 0.49	0.53 ± 0.07
1	0.165 ± 0.001	2.30 ± 0.25	0.34 ± 0.05
3	0.168 ± 0.001	2.10 ± 0.1	0.32 ± 0.01
5	0.146 ± 0.002	2.40 ± 0.1	0.33 ± 0.01

higher filler concentrations, tend to limit the positive thermal conductivity effect of the presence of NDs.

In Figure 8, the mass loss curves of PEX and its nanocomposites with NDs are presented, revealing a thermal



**Figure 8.** Mass loss curves of PEX and its composites with 0–5 wt % NDs.

stability enhancement of 8–9 °C for the composite with the lowest amount of fillers. The other three composites have almost the same mass loss behavior as neat PEX. The thermal stability enhancement is a commonly observed phenomenon in polymer nanocomposites<sup>82,83</sup> and can be justified in the framework of nanoconfinement. More specifically, it has been proven that the nanofillers (dispersed or aggregated) form nanoconfined regions in the bulk of the matrix around which the macromolecular chains cannot maintain their regular coil conformation.<sup>84</sup> Moreover, in the nanoconfined areas, the chain mobility is found to be hindered, resulting in changes in the molecular transition dynamics.<sup>84</sup> The hindered chain mobility leads to lower chemical reactivity, and therefore enhanced thermal stability in these systems.

In the present case, it seems that smaller amounts of more adequately dispersed nanofillers create more nanoconfined regions than those created for the higher filler loadings. Therefore, the restricted chain mobility and hindered chain dynamics are more effective in the composites with lower filler content, and thus in these composites the thermal stability is more enhanced.

To confirm the TG findings, py-GC–MS experiments were also performed at 420 °C corresponding to the initial mass loss steps of the composites. The obtained chromatograms are presented in Figure 9, confirming the thermogravimetric findings. The gaseous products evolving during the first 5 min of PEX's decomposition (marked as area 1 in Figure 9) are water, ethylene, and propane ( $m/z$ : 18, 28, 44), while, as reported previously,<sup>19</sup> between 5 and 12 min of retention, light polyethylene decomposition fragments along with some polysiloxanes are also collected ( $m/z$  281, 355, 341) (area 2 in Figure 9). From that point on, linear hydrocarbons (containing 7–35 carbons) were collected in a typical polyethylene decomposition pattern (area 3 in Figure 9).

As found through the thermogravimetric studies, the presence of NDs seems to enhance the thermal stability of PEX mainly in low concentrations. The clear difference in the chromatograms of the composite with 0.5 wt % NDs as compared to the neat polymer confirms its superior thermal stability. The integral intensity of the collected products is

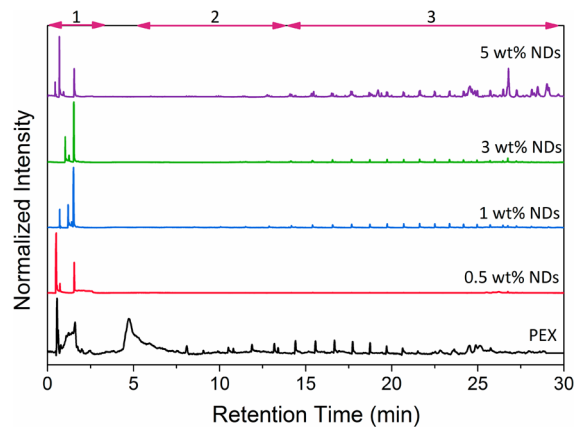


**Figure 9.** Pyrolysis chromatograms of PEX and its composites with 0–5 wt % NDs.

significantly lower than the corresponding one of PEX. The chromatograms of the other composites present progressively higher integral intensities and a tendency to yield the same gaseous decomposition products as the neat polymer. The most intense peaks of the chromatograms of all nanocomposites were recorded during the initial 2 min of retention and correspond to water, ethylene, and propane in all cases. Therefore, the most intense gaseous decomposition fragments were the same as in neat polymer. However, the reactions involved during chain scission and fragmentation of polyethylene giving rise to the various linear hydrocarbons could not so easily progress in the presence of NDs. This can be associated with the presence of nanoconfined areas induced by the nanofillers as previously stressed. Thus, a thermal stability enhancement on the low NDs concentrations was associated with the more effectively hindered chain dynamics of these composites.

It is noteworthy that both mechanical and thermal properties are more significantly enhanced in the low NDs concentration composites, while they all tend to decrease with increasing filler content, even though they are fundamentally influenced by different factors.

#### 4. CONCLUSIONS

PEX nanocomposites with small amounts of NDs were prepared by solid-state ball milling and subsequent melt-mixing and were found to have greatly enhanced mechanical and thermal properties. The mechanical properties of the composites were thoroughly examined and were found to be influenced by crystal structure, molecular conformation, filler dispersion, filler–matrix interactions, and adhesion. It was detected that the strength, toughness, and elastic modulus of the composites were significantly enhanced in the composites with low filler content (up to 1 wt %). For higher NDs concentrations, the composites' properties degraded.

When filler concentration does not exceed 1 wt %, quite small NDs aggregates are formed, while an overall fine dispersion is achieved and adhesion is very high. Moreover, crystallinity and crystal size were notably higher in these composites, allowing the successful reinforcement of the matrix. Higher filler concentrations lead to lower crystallinity enhancement level and similarly sized or even smaller crystals. Also, the filler aggregates were found to be larger and with lower adhesion with the matrix resulting in its inferior reinforcement. These findings were consistent with the fractography

observations. The aggregates formed in higher filler concentrations act as stress concentrators prohibiting the load carrying over the formed cracks, and thus leading to lower toughness and premature failure.

Regarding the significantly enhanced thermal conductivity of the composites, it was found that it mainly resulted from the heat capacity increase that the presence of NDs induced. This enhancement is much more significant in the composite with the lowest filler concentration in which the higher filler dispersion, adhesion, and interactions were observed. The similar finding in the thermal stability of the composites confirms that the incorporation of a smaller amount of particles, which leads to better dispersion and adhesion, is the key to successful property reinforcement of these materials.

## ASSOCIATED CONTENT

### Supporting Information

FTIR spectrum of the as-received nanodiamonds particles. This material is available free of charge via the Internet at <http://pubs.acs.org>.

## AUTHOR INFORMATION

### Corresponding Authors

\*E-mail: eroumeli@auth.gr.

\*E-mail: hrisafis@physics.auth.gr.

### Notes

The authors declare no competing financial interest.

## ACKNOWLEDGMENTS

We would like to thank Prof. Aldo Boccaccini of the University of Erlangen-Nürnberg for allowing the contact angle measurements on the facilities available at Biomaterials Department. We would also like to thank assoc. prof. Th. Kyratsi for allowing the thermal diffusivity measurements in the facilities of the Mechanical and Manufacturing Engineering Department of the University of Cyprus. We wish to acknowledge cofunding of this research by European Union-European Regional Development Fund and Greek Ministry of Education/EYDE-ETAK through program ESPA 2007-2013/EPAN II/Action "SYNERGASIA" (project 09SYN-33-484).

## REFERENCES

- (1) Vaia, R. A.; Wagner, H. D. Framework for Nanocomposites. *Mater. Today* **2004**, *7*, 32–37.
- (2) Bansal, A.; Yang, H.; Li, C.; Cho, K.; Benicewicz, B. C.; Kumar, S. K.; Schadler, L. S. Quantitative Equivalence between Polymer Nanocomposites and Thin Polymer Films. *Nat. Mater.* **2005**, *4*, 693–698.
- (3) Darras, O.; Séguéla, R. Tensile Yield of Polyethylene in Relation to Crystal Thickness. *J. Phys. Chem. B* **1993**, *31*, 759–766.
- (4) Galeski, A.; Bartczak, Z.; Kazmierczak, T.; Slouf, M. Morphology of Undeformed and Deformed Polyethylene Lamellar Crystals. *Polymer* **2010**, *51*, 5780–5787.
- (5) Schrauwen, B. A. G.; Janssen, R. P. M.; Govaert, L. E.; Meijer, H. E. H. Intrinsic Deformation Behavior of Semicrystalline Polymers. *Macromolecules* **2004**, *37*, 6069–6078.
- (6) Schultz, J. M. Microstructural Aspects of Failure in Semicrystalline Polymers. *Polym. Eng. Sci.* **1984**, *24*, 770–785.
- (7) Zhou, L.; Gao, C.; Xu, W. Simultaneous Photoluminescence Import and Mechanical Enhancement of Polymer Films Using Silica-Hybridized Quantum Dots. *J. Mater. Chem.* **2010**, *20*, 5675–5681.
- (8) Lee, M. C. H. Effects of Polymer-Filler Adhesion on the Properties of Polychloroprene Elastomers Filled with Surface-Treated Fillers. *J. Appl. Polym. Sci.* **1987**, *33*, 2479–2492.
- (9) Fu, S.-Y.; Feng, X.-Q.; Lauke, B.; Mai, Y.-W. Effects of Particle Size, Particle/Matrix Interface Adhesion and Particle Loading on Mechanical Properties of Particulate–Polymer Composites. *Composites, Part B* **2008**, *39*, 933–961.
- (10) Krishnamoorti, R.; Vaia, R. A.; Giannelis, E. P. Structure and Dynamics of Polymer-Layered Silicate Nanocomposites. *Chem. Mater.* **1996**, *8*, 1728–1734.
- (11) Giannelis, E. P. Polymer-Layered Silicate Nanocomposites: Synthesis, Properties and Applications. *Appl. Organomet. Chem.* **1998**, *12*, 675–680.
- (12) Liu, C.; Ma, J.; Gan, X.; Li, R.; Wang, J. Effects of Organic Chain Length of Layered Zirconium Phosphonate on the Structure and Properties of Castor Oil-Based Polyurethane Nanocomposites. *Compos. Sci. Technol.* **2012**, *72*, 915–923.
- (13) Tjong, S. C. Polymer Nanocomposite Bipolar Plates Reinforced with Carbon Nanotubes and Graphite Nanosheets. *Energy Environ. Sci.* **2011**, *4*, 605–626.
- (14) Wang, M. H.; Ruan, W. H.; Huang, Y. F.; Ye, L.; Rong, M. Z.; Zhang, M. Q. A Strategy for Significant Improvement of Strength of Semi-Crystalline Polymers with the Aid of Nanoparticles. *J. Mater. Chem.* **2012**, *22*, 4592–4598.
- (15) Tsunaga, M.; Matsunami, S.; Sato, M.; Nakata, K. Crosslinked Polyethylene Pipe for Hot Water and Geothermal Applications. *Plast., Rubber Compos.* **1998**, *27*, 460–464.
- (16) Khonakdar, H. A.; Morshedian, J.; Wagenknecht, U.; Jafari, S. H. An Investigation of Chemical Crosslinking Effect on Properties of High-Density Polyethylene. *Polymer* **2003**, *44*, 4301–4309.
- (17) Oliveira, G. L.; Costa, M. F. Optimization of Process Conditions, Characterization and Mechanical Properties of Silane Crosslinked High-Density Polyethylene. *Mater. Sci. Eng., A* **2010**, *527*, 4593–4599.
- (18) Roumeli, E.; Pavlidou, E.; Bikaris, D.; Chrissafis, K. Microscopic Observation and Micromechanical Modeling to Predict the Enhanced Mechanical Properties of Multi-Walled Carbon Nanotubes Reinforced Crosslinked High Density Polyethylene. *Carbon* **2014**, *67*, 475–487.
- (19) Roumeli, E.; Markoulis, A.; Kyratsi, T.; Bikaris, D.; Chrissafis, K. Carbon Nanotube-Reinforced Crosslinked Polyethylene Pipes for Geothermal Applications: From Synthesis to Decomposition Using Analytical Pyrolysis–Gc/Ms and Thermogravimetric Analysis. *Polym. Degrad. Stab.* **2014**, *100*, 42–53.
- (20) Pech, D.; Brunet, M.; Durou, H.; Huang, P.; Mochalin, V.; Gogotsi, Y.; Taberna, P.-L.; Simon, P. Ultrahigh-Power Micrometre-Sized Supercapacitors Based on Onion-Like Carbon. *Nat. Nano* **2010**, *5*, 651–654.
- (21) Mochalin, V. N.; Shenderova, O.; Ho, D.; Gogotsi, Y. The Properties and Applications of Nanodiamonds. *Nat. Nano* **2012**, *7*, 11–23.
- (22) Lai, L.; Barnard, A. S. Modeling the Thermostability of Surface Functionalisation by Oxygen, Hydroxyl, and Water on Nanodiamonds. *Nanoscale* **2011**, *3*, 2566–2575.
- (23) Maitra, U.; Prasad, K. E.; Ramamurty, U.; Rao, C. N. R. Mechanical Properties of Nanodiamond-Reinforced Polymer-Matrix Composites. *Solid State Commun.* **2009**, *149*, 1693–1697.
- (24) Behler, K. D.; Stravato, A.; Mochalin, V.; Korneva, G.; Yushin, G.; Gogotsi, Y. Nanodiamond-Polymer Composite Fibers and Coatings. *ACS Nano* **2009**, *3*, 363–369.
- (25) Dolmatov, V. Y. Detonation Nanodiamonds in Oils and Lubricants. *J. Superhard Mater.* **2010**, *32*, 14–20.
- (26) Neitzel, I.; Mochalin, V.; Knoke, I.; Palmese, G. R.; Gogotsi, Y. Mechanical Properties of Epoxy Composites with High Contents of Nanodiamond. *Compos. Sci. Technol.* **2011**, *71*, 710–716.
- (27) Voznyakovskii, A. P.; Ginzburg, B. M.; Rashidov, D.; Tochil'nikov, D. G.; Tuichiev, S. Structure, Mechanical, and Tribological Characteristics of Polyurethane Modified with Nanodiamonds. *Polym. Sci., Ser. A* **2010**, *52*, 1044–1050.
- (28) Ayatollahi, M. R.; Alishahi, E.; Doagou-R, S.; Shadlou, S. Tribological and Mechanical Properties of Low Content Nanodiamond/Epoxy Nanocomposites. *Composites, Part B* **2012**, *43*, 3425–3430.

- (29) Rakha, S. A.; Jianqing, C.; Huihao, X.; Guojun, Y.; Zhu, D.; Gong, J. Incorporation of Hydrogen in Diamond Thin Films. *Diamond Relat. Mater.* **2009**, *18*, 1247–1252.
- (30) Shakun, A.; Vuorinen, J.; Hoikkanen, M.; Poikelispää, M.; Das, A. Hard Nanodiamonds in Soft Rubbers: Past, Present and Future – a Review. *Composites, Part. A* **2014**, *64*, 49–69.
- (31) Neitzel, I.; Mochalin, V.; Gogotsi, Y. Chapter 13 – Advances in Surface Chemistry of Nanodiamond and Nanodiamond–Polymer Composites. In *Ultrananocrystalline Diamond: Synthesis, Properties and Applications*; Shenderova, O. A., Gruen, D. M., Eds.; Elsevier Science: New York, 2012; pp 421–456.
- (32) Krueger, A.; Lang, D. Functionality Is Key: Recent Progress in the Surface Modification of Nanodiamond. *Adv. Funct. Mater.* **2012**, *22*, 890–906.
- (33) Neitzel, I.; Mochalin, V. N.; Niu, J.; Cuadra, J.; Kontsos, A.; Palmese, G. R.; Gogotsi, Y. Maximizing Young's Modulus of Aminated Nanodiamond-Epoxy Composites Measured in Compression. *Polymer* **2012**, *53*, 5965–5971.
- (34) Chang, I. P.; Hwang, K. C.; Ho, J.-a. A.; Lin, C.-C.; Hwu, R. J. R.; Horng, J.-C. Facile Surface Functionalization of Nanodiamonds. *Langmuir* **2009**, *26*, 3685–3689.
- (35) Williams, O. A.; Hees, J.; Dieker, C.; Jäger, W.; Kirste, L.; Nebel, C. E. Size-Dependent Reactivity of Diamond Nanoparticles. *ACS Nano* **2010**, *4*, 4824–4830.
- (36) Shenderova, O.; Jones, C.; Borjanovic, V.; Hens, S.; Cunningham, G.; Moseenkov, S.; Kuznetsov, V.; McGuire, G. Detonation Nanodiamond and Onion-Like Carbon: Applications in Composites. *Phys. Status Solidi A* **2008**, *205*, 2245–2251.
- (37) Kruger, A.; Liang, Y.; Jarre, G.; Stegk, J. Surface Functionalisation of Detonation Diamond Suitable for Biological Applications. *J. Mater. Chem.* **2006**, *16*, 2322–2328.
- (38) Zhang, Q.; Mochalin, V. N.; Neitzel, I.; Knoke, I. Y.; Han, J.; Klug, C. A.; Zhou, J. G.; Lelkes, P. I.; Gogotsi, Y. Fluorescent Pilla-Nanodiamond Composites for Bone Tissue Engineering. *Biomaterials* **2011**, *32*, 87–94.
- (39) Ohtani, B.; Kim, Y.-h.; Yano, T.; Hashimoto, K.; Fujishima, A.; Uosaki, K. Surface Functionalization of Doped Cvd Diamond Via Covalent Bond. An Xps Study on the Formation of Surface-Bound Quaternary Pyridinium Salt. *Chem. Lett.* **1998**, *27*, 953–954.
- (40) Nichols, B. M.; Butler, J. E.; Russell, J. N.; Hamers, R. J. Photochemical Functionalization of Hydrogen-Terminated Diamond Surfaces: A Structural and Mechanistic Study. *J. Phys. Chem. B* **2005**, *109*, 20938–20947.
- (41) Zhuang, H.; Srikanth, V. V. S. S.; Jiang, X.; Aronov, I.; Wenclawiak, B. W.; Luo, J.; Ihmels, H. Elucidation of Different Steps Involved in Allylamine Functionalization of the Diamond Surface and Its Polymerization by Time-of-Flight Secondary Ion Mass Spectrometry. *Chem. Mater.* **2010**, *22*, 4414–4418.
- (42) Rezek, B.; Shin, D.; Nakamura, T.; Nebel, C. E. Geometric Properties of Covalently Bonded DNA on Single-Crystalline Diamond. *J. Am. Chem. Soc.* **2006**, *128*, 3884–3885.
- (43) Amemiya, Y.; Hatakeyama, A.; Shimamoto, N. Aminosilane Multilayer Formed on a Single-Crystalline Diamond Surface with Controlled Nanoscopic Hardness and Bioactivity by a Wet Process. *Langmuir* **2008**, *25*, 203–209.
- (44) Perevedentseva, E.; Cai, P. J.; Chiu, Y. C.; Cheng, C. L. Characterizing Protein Activities on the Lysozyme and Nanodiamond Complex Prepared for Bio Applications. *Langmuir* **2010**, *27*, 1085–1091.
- (45) Lee, J. W.; Lee, S.; Jang, S.; Han, K. Y.; Kim, Y.; Hyun, J.; Kim, S. K.; Lee, Y. Preparation of Non-Aggregated Fluorescent Nanodiamonds (FnDs) by Non-Covalent Coating with a Block Copolymer and Proteins for Enhancement of Intracellular Uptake. *Mol. BioSyst.* **2013**, *9*, 1004–1011.
- (46) Fu, C.-C.; Lee, H.-Y.; Chen, K.; Lim, T.-S.; Wu, H.-Y.; Lin, P.-K.; Wei, P.-K.; Tsao, P.-H.; Chang, H.-C.; Fann, W. Characterization and Application of Single Fluorescent Nanodiamonds as Cellular Biomarkers. *Proc. Natl. Acad. Sci. U.S.A.* **2007**, *104*, 727–732.
- (47) Boudou, J.-P.; Curmi, P. A.; Jelezko, F.; Wrachtrup, J.; Aubert, P.; Sennour, M.; Balasubramanian, G.; Reuter, R.; Thorel, A.; Gaffet, E. High Yield Fabrication of Fluorescent Nanodiamonds. *Nanotechnology* **2009**, *20*, 235602.
- (48) Balasubramanian, G.; et al. Nanoscale Imaging Magnetometry with Diamond Spins under Ambient Conditions. *Nature* **2008**, *455*, 648–651.
- (49) Lam, R.; Chen, M.; Pierstorff, E.; Huang, H.; Osawa, E.; Ho, D. Nanodiamond-Embedded Microfilm Devices for Localized Chemo-therapeutic Elution. *ACS Nano* **2008**, *2*, 2095–2102.
- (50) Kossovsky, N.; Gelman, A.; Hnatyszyn, H. J.; Rajguru, S.; Garrell, R. L.; Torbati, S.; Freitas, S. S. F.; Chow, G.-M. Surface-Modified Diamond Nanoparticles as Antigen Delivery Vehicles. *Bioconjugate Chem.* **1995**, *6*, 507–511.
- (51) Jee, A.-Y.; Lee, M. Thermal and Mechanical Properties of Alkyl-Functionalized Nanodiamond Composites. *Curr. Appl. Phys.* **2011**, *11*, 1183–1187.
- (52) Pentecost, A.; Gour, S.; Mochalin, V.; Knoke, I.; Gogotsi, Y. Deaggregation of Nanodiamond Powders Using Salt- and Sugar-Assisted Milling. *ACS Appl. Mater. Interfaces* **2010**, *2*, 3289–3294.
- (53) Osawaa, E.; Sasakib, S.; Yamanoia, R. In *Ultrananocrystalline Diamond: Synthesis, Properties and Applications*; Shenderova, O. A., Gruen, D. M., Eds.; Elsevier Science: New York, 2012; Chapter 6.
- (54) Enqvist, E.; Emami, N. Nanodiamond Reinforced Ultra High Molecular Weight Polyethylene for Orthopaedic Applications: Dry Versus Wet Ball Milling Manufacturing Methods. *Tribologia* **2014**, *8*, 7–13.
- (55) Ozawa, M.; Inaguma, M.; Takahashi, M.; Kataoka, F.; Krüger, A.; Ōsawa, E. Preparation and Behavior of Brownish, Clear Nanodiamond Colloids. *Adv. Funct. Mater.* **2007**, *19*, 1201–1206.
- (56) Attia, N. F.; Rao, J. P.; Geckeler, K. E. Nanodiamond–Polymer Nanoparticle Composites and Their Thin Films. *J. Nanopart. Res.* **2014**, *16*, 1–12.
- (57) Roumelis, E.; Paraskevopoulos, K. M.; Bikaris, D.; Chrissafis, K. Effect of High Energy Ball Milling on the Structure and Mechanical Properties of Cross-Linked High Density Polyethylene. *J. Mater. Sci.* **2013**, *48*, 6753–6761.
- (58) Ebewele, R. O. *Polymer Science and Technology*; Taylor & Francis: UK, 2000.
- (59) Morimune, S.; Kotera, M.; Nishino, T.; Goto, K.; Hata, K. Poly(Vinyl Alcohol) Nanocomposites with Nanodiamond. *Macromolecules* **2011**, *44*, 4415–4421.
- (60) Korobko, A. P.; Bessonova, N. P.; Krasheninnikov, S. V.; Konyukhova, E. V.; Drozd, S. N.; Chvalun, S. N. Nanodiamonds as Modifier of Ethylene-1-Octene Copolymer Structure and Properties. *Diamond Relat. Mater.* **2007**, *16*, 2141–2144.
- (61) Zhao, Y.-Q.; Lau, K.-T.; Kim, J.-k.; Xu, C.-L.; Zhao, D.-D.; Li, H.-L. Nanodiamond/Poly (Lactic Acid) Nanocomposites: Effect of Nanodiamond on Structure and Properties of Poly (Lactic Acid). *Composites, Part B* **2010**, *41*, 646–653.
- (62) Roesler, J.; Harders, H.; Baeker, M. *Mechanical Behaviour of Engineering Materials: Metals, Ceramics, Polymers, and Composites*; Springer: New York, 2007.
- (63) Zhang, L.; Tian, G.; Wang, X.; Qi, S.; Wu, Z.; Wu, D. Polyimide/Ladder-Like Polysilsesquioxane Hybrid Films: Mechanical Performance, Microstructure and Phase Separation Behaviors. *Composites, Part B* **2014**, *56*, 808–814.
- (64) Young, T. An Essay on the Cohesion of Fluids. *Philos. Trans. R. Soc., A* **1805**, *95*, 65–87.
- (65) Wu, S. Calculation of Interfacial Tension in Polymer Systems. *J. Polym. Sci., Part C: Polym. Symp.* **1971**, *34*, 19.
- (66) Owens, D. K.; Wendt, R. C. Estimation of the Surface Free Energy of Polymers. *J. Appl. Polym. Sci.* **1969**, *13*, 1741–1747.
- (67) de Gennes, P. G. Wetting: Statics and Dynamics. *Rev. Mod. Phys.* **1985**, *57*, 827–863.
- (68) Cooper, W. F.; Nuttall, W. H. The Theory of Wetting, and the Determination of the Wetting Power of Dipping and Spraying Fluids Containing a Soap Basis. *J. Agric. Sci.* **1915**, *7*, 219–239.

- (69) Girifalco, L. A.; Good, R. J. A Theory for the Estimation of Surface and Interfacial Energies. I. Derivation and Application to Interfacial Tension. *J. Phys. Chem.* **1957**, *61*, 904–909.
- (70) Tanniru, M.; Yuan, Q.; Misra, R. D. K. On Significant Retention of Impact Strength in Clay-Reinforced High-Density Polyethylene (Hdpe) Nanocomposites. *Polymer* **2006**, *47*, 2133–2146.
- (71) Rizzo, P.; Baione, F.; Guerra, G.; Martinotto, L.; Albizzati, E. Polyethylene Unit Cell and Crystallinity Variations as a Consequence of Different Cross-Linking Processes. *Macromolecules* **2001**, *34*, 5175–5179.
- (72) Bunn, C. W. The Crystal Structure of Long-Chain Normal Paraffin Hydrocarbons. The “Shape” of the <math>\text{Ch}\_2</math> Group. *Trans. Faraday Soc.* **1939**, *35*, 482–491.
- (73) Hermans, P. H.; Weidinger, A. On the Determination of the Crystalline Fraction of Polyethylenes from X-Ray Diffraction. *Makromol. Chem.* **1961**, *44*, 24–36.
- (74) Papageorgiou, D. G.; Vourlias, G.; Bikaris, D. N.; Chrissafis, K. Synergistic Effect of Functionalized Silica Nanoparticles and a B-Nucleating Agent for the Improvement of the Mechanical Properties of a Propylene/Ethylene Random Copolymer. *Macromol. Mater. Eng.* **2013**.
- (75) Way, J. L.; Atkinson, J. R.; Nutting, J. The Effect of Spherulite Size on the Fracture Morphology of Polypropylene. *J. Mater. Sci.* **1974**, *9*, 293–299.
- (76) Wunderlich, B. *Macromolecular Physics: Crystal Nucleation, Growth, Annealing*; Academic Press: New York, 1976.
- (77) Hoffman, J. D. Role of Reptation in the Rate of Crystallization of Polyethylene Fractions from the Melt. *Polymer* **1982**, *23*, 656–670.
- (78) Wunderlich, B.; Czornyj, G. A Study of Equilibrium Melting of Polyethylene. *Macromolecules* **1977**, *10*, 906–913.
- (79) Krook, M.; Hedenqvist, M. S.; Albertsson, A. C.; Hellman, A.; Iversen, T.; Gedde, U. W. Barrier and Mechanical Properties of Pulp Fiber/Polymer Laminates and Blends. *Polym. Eng. Sci.* **2000**, *40*, 143–156.
- (80) Wunderlich, B. *Thermal Analysis of Polymeric Materials*; Springer: New York, 2005.
- (81) Tsuji, H.; Aratani, T.; Takikawa, H. Physical Properties, Crystallization, and Thermal/Hydrolytic Degradation of Poly(L-Lactide)/Nano/Micro-Diamond Composites. *Macromol. Mater. Eng.* **2013**, *298*, 1149–1159.
- (82) Chrissafis, K.; Bikaris, D. Can Nanoparticles Really Enhance Thermal Stability of Polymers? Part I: An Overview on Thermal Decomposition of Addition Polymers. *Thermochim. Acta* **2011**, *523*, 1–24.
- (83) Bikaris, D. Can Nanoparticles Really Enhance Thermal Stability of Polymers? Part II: An Overview on Thermal Decomposition of Polycondensation Polymers. *Thermochim. Acta* **2011**, *523*, 25–45.
- (84) Chen, K.; Wilkie, C. A.; Vyazovkin, S. Nanoconfinement Revealed in Degradation and Relaxation Studies of Two Structurally Different Polystyrene–Clay Systems. *J. Phys. Chem. B* **2007**, *111*, 12685–12692.